

000
001
002
003
004
005
006
007
008
009
010
011
012
013
014
015054
055
056
057
058
059
060
061
062
063
064
065
066
067
068
069
070
071
072
073
074
075
076
077
078
079
080
081
082
083
084
085
086
087
088
089
090
091
092
093
094
095
096
097
098
099
100
101
102
103
104
105
106
107

External Patch Group Prior Guided Internal Orthogonal Dictionary Learning for Real Image Denoising

Anonymous CVPR submission

Paper ID ****

Abstract

For image denoising problem, the external and internal priors are playing key roles in many different methods. External priors learn from external images to restore noisy images while internal ones exploit priors of given images for denoising. The external priors are more generative and efficient on recovering structures existing in most images while the internal priors are more adaptive on recovering details existed in given noisy images. In this paper, we propose to employ the external patch group prior of images to guide the clustering of internal patch groups, and develop an external dictionary guided internal orthogonal dictionary learning algorithm for real image denoising. The internal orthogonal dictionary learning process has closed-form solutions and hence very efficient for online denoising. The experiments on standard datasets demonstrate that, that the proposed method achieves much better denoising performance than the other state-of-the-art methods on real image denoising.

1. Introduction

Most vision systems, such as medical imaging and surveillance, need accurate feature extraction from high-quality images. The camera sensors and outdoor low light conditions will unavoidly bring noise to the captured images. The impact is that the image details will be lost or hardly visible. As a result, image denoising is an essential procedure for the reliability of these vision systems. In the research area, image denoising is also an ideal platform for testing natural image models and provides high-quality images for other computer vision tasks such as image registration, segmentation, and pattern recognition, etc.

For several decades, there emerge numerous image denoising methods [1, 2, 3, 4, 5, 6, 7, 8, 9, 10, 11], and all of them focus mainly on dealing with additive white Gaussian noise (AWGN). In real world, the cameras will undertake high ISO settings for high-speed shots on actions,

long exposure for low light on night shots, etc. Under these situations, the noise is generated in a complex form and also been changed during the in-camera imaging pipeline [12, 13]. Therefore, the noise in real images are much more complex than Gaussian [13, 24]. It depends on camera series, brands, as well as the settings (ISO, shutter speed, and aperture, etc). The models designed for AWGN would become much less effective on real noisy images.

In the last decade, the methods of [14, 15, 16, 17, 18, 19, 13] are developed to deal with real noisy images. Almost all these methods employ a two-stage framework: estimating the parameters of the assumed noise model (usually Gaussian) and performing denoising with the help of the noise modeling and estimation in the first stage. However, the Gaussian assumption is inflexible in describing the complex noise on real noisy images [16]. Although the mixture of Gaussians (MoG) model is possible to approximate any noise distribution [20], estimating its parameters is time consuming via nonparametric Bayesian techniques [19]. To evaluate the performance of these methods on dealing with complex real noise, we apply these methods, with corresponding default parameters, on a real noisy image provided in [13]. The testing image is captured by a Nikon D800 camera when ISO is 3200. The "ground truth" image is also provided with which we can calculate objective measurements such as PSNR and SSIM [21]. The denoised images are listed in Figure 1, from which we can see that these methods either remove the noise or oversmooth the complex details in real noisy image.

The above mentioned methods can be categorized into external methods which learn priors from external images to recover noisy images, and internal ones which exploit priors of given images for denoising. The external priors in natural images are free of the high correlation between noise and signals in real noisy images, while the internal prior is adaptive to the image and can recover better the latent clean image. Combining the priors of external clean images and adaptively of internal testing images can naturally improve the performance of denoising methods, especially on real noisy images. Based on these observations, in this paper,

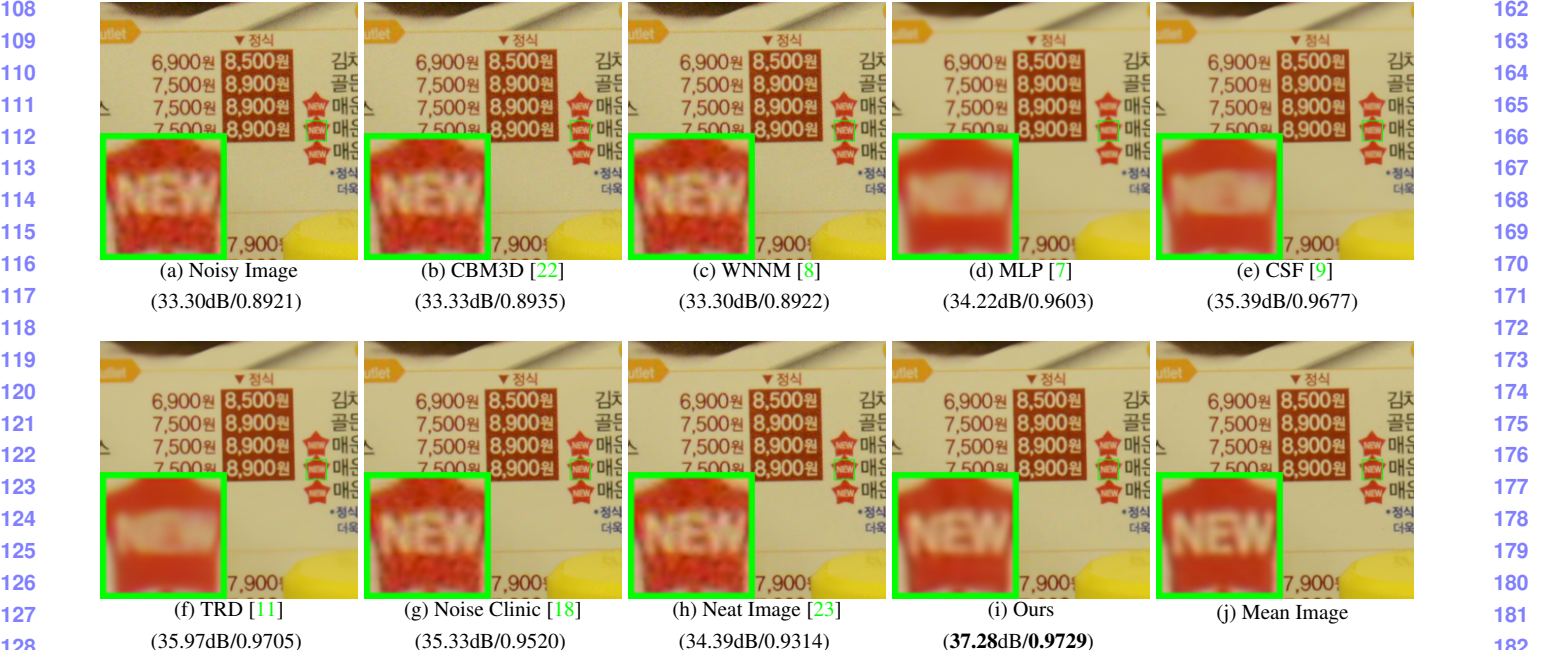


Figure 1. Denoised images of the real noisy image "NikonD800ISO3200A3" by different methods. The images are better to be zoomed on screen.

we propose to employ the external patch group prior [10] of natural clean images to guide the clustering of internal patch groups in given noisy image, and develop an external prior guided internal orthogonal dictionary learning (DL) algorithm for real image denoising. The internal orthogonal DL process includes two alternating stages: updating sparse coefficients and updating orthogonal dictionary. Both of the two stages have closed-form solutions. Hence, our internal DL process is very efficient for online internal denoising.

1.1. Our Contributions

The contributions of this paper are summarized as follows:

- We propose a novel method which combine the external and internal PG prior for real noisy image denoising problem;
- Our method doesn't need noise modeling and estimation, and the noise levels of real noisy images are automatically expressed by the singular values of learned subspace;
- We achieve much better performance on visual quality, PSNR, SSIM, and speed, than other competing methods for real image denoising problem.

The rest of this paper will be summarized as follows: in Section 2, we will introduce the related work close to our work; in Section 3, we will introduce our proposed external prior guided internal subspace learning framework for real

image denoising; in Section 4, we will demonstrate the denoising experiments on several standard dataset; in Section 5, we will conclude our paper and give our future work.

2. Related Work

2.1. Patch Group Prior of Natural Images

The Patch Group (PG) prior [10] is proposed to directly model the non-local self similar (NSS) property of natural images. The NSS property is commonly used in image restoration tasks [1, 4, 5, 8, 10]. The PG prior largely reduces the space of images to be modeled when compared to the patch prior [6]. The better modeling on NSS is demonstrated via better image denoising performance on natural images. However, in [10], only the PGs of clean natural images is utilized, while the PGs of noisy input images are ignored. In this paper, we aim at making use of both PGs from natural clean images and real noisy images for better denoising performance.

2.2. Internal v.s. External Dictionary Learning

For natural images, the internal patch recurrence across multiple scales has been successfully applied in many image restoration problems [25, 26, 27, 28]. These work demonstrate that internal information is enough for many ill-posed problems including denoising additive white Gaussian noise. The rationale is, since the AWGN noise is independent of the original clean images, it will be reduced if the image is scaled to a smaller size. However, the noise

in real images is generated mostly from the camera sensors, which is highly complex and signal dependent [13]. Besides, according to the seminar workd of [24], the noise in real images has fixed patterns from several main sources. Therefore, we can hardly seperate the complex noise from the signals without the help of external (correct) information of natural clean images. Only using the internal information may be not enough for real image denoising problem. On the other hand, the methods only using the external information may be not adaptive for real noisy images. Recently, the methods of [7, 9, 11] had been proposed to learn, on both internal and external images, a process directly mapping the noisy patches to denoised ones. These discriminative learning based methods are only effective on additive white Gaussian noise and ineffective on complex and signal dependent noise in real images. This has been shown in Figure 1. In this paper, our goal is to make use of external information to guide the subspace learning of internal PGs for image denoising task.

2.3. Real Image Denoising

To the best of our knowledge, the study of real image denoising can be dated back to the BLS-GSM model [29], in which Portilla et al. proposed to use scale mixture of Gaussian in overcomplete oriented pyramids to estimate the latent clean images. In [14], Portilla proposed to use a correlated Gaussian model for noise estimation of each wavelet subband. Based on the robust statistics theory [30], the work of Rabie [15] modeled the noisy pixels as outliers, which could be removed via Lorentzian robust estimator. In [16], Liu et al. proposed to use ‘noise level function’ (NLF) to estimate the noise and then use Gaussian conditional random field to obtain the latent clean image. Recently, Gong et al. proposed an optimization based method [17], which models the data fitting term by weighted sum of ℓ_1 and ℓ_2 norms and the regularization term by sparsity prior in the wavelet transform domain. Later, Lebrun el al. proposed a multiscale denoising algorithm called ‘Noise Clinic’ [18] for real image denoising task. This method generalizes the NL-Bayes [31] to deal with signal, scale, and frequency dependent noise. Recently, Zhu et al. proposed a Bayesian model [19] which approximates the noise via Mixture of Gaussian (MoG) model [20]. The clean image is recovered from the noisy image by the proposed Low Rank MoG filter (LR-MoG). In this paper, we proposed a noval denoising method achieving much better performance than previous real denoising methods.

3. External Patch Group Prior Guided Internal Orthogonal Dictionary Learning

In this section, we formulate the framework of external Patch Group prior guided internal subspace learning. We first introduce the patch group prior leaning on clean natural

RGB images. Then we formulate the external guided internal subspace learning. Finally, we discuss the differences between external subspaces and the corresponding internal subspace.

3.1. External Patch Group Prior Learning

Natural images often demonstrate repepitve patterns, this nonlocal self-similarity (NSS) property is a key successful factor for many image denoising methods [1, 4, 5, 32, 8, 10] and restoration methods []. In [10], the NSS property is directly learned as an external prior in a patch group manner. In this section, we formulate the Patch Group prior on natural color images.

In [10], the patch group (PG) is defined as a group of similar patches to the local patch. The patch group mean is dstracted, and hence different groups patches can share similar PGs. Therefore the space to be modeled is largely reduced. In this work, we extract PGs from RGB images. Each patch is of size $p \times p \times 3$. For each local patch, we search its similar patches around it through the Euclidean distance in a local window of size $W \times W$. The PG is denoted by $\{\mathbf{x}_m\}_{m=1}^M$, where $\mathbf{x}_m \in \mathbb{R}^{3p^2 \times 1}$ is a color image patch vector. The mean vector of this PG is $\boldsymbol{\mu} = \frac{1}{M} \sum_{m=1}^M \mathbf{x}_m$, and $\bar{\mathbf{x}}_m = \mathbf{x}_m - \boldsymbol{\mu}$ is the group mean subtracted patch vector. The PG is defined as $\bar{\mathbf{X}} \triangleq \{\bar{\mathbf{x}}_m\}, m = 1, \dots, M$, and it represent the external NSS prior on color images. Assume we have extracted N PGs from a given set of natural images, and the n -th PG is defined as $\bar{\mathbf{X}}_n \triangleq \{\bar{\mathbf{x}}_{n,m}\}_{m=1}^M, n = 1, \dots, N$. We employ the patch group based Gaussian Mixture Model (PG-GMM) for NSS prior learning. We aim to learn a set of K Gaussians $\{\mathcal{N}(\boldsymbol{\mu}_k, \Sigma_k)\}$ from N training PGs $\{\bar{\mathbf{X}}_n\}$, while requiring that all the M patches $\{\bar{\mathbf{x}}_{n,m}\}$ in PG $\bar{\mathbf{X}}_n$ belong to the same Gaussian component and assume that the patches in the PG are independently sampled. Note that such an assumption is commonly used in patch based image modeling [3, 5]. Then, the likelihood of $\{\bar{\mathbf{X}}_n\}$ can be calculated as

$$P(\bar{\mathbf{X}}_n) = \sum_{k=1}^K \pi_k \prod_{m=1}^M \mathcal{N}(\bar{\mathbf{x}}_{n,m} | \boldsymbol{\mu}_k, \Sigma_k). \quad (1)$$

By assuming that all the PGs are independently sampled, the overall objective log-likelihood function is

$$\ln \mathcal{L} = \sum_{n=1}^N \ln \left(\sum_{k=1}^K \pi_k \prod_{m=1}^M \mathcal{N}(\bar{\mathbf{x}}_{n,m} | \boldsymbol{\mu}_k, \Sigma_k) \right). \quad (2)$$

We maximize the above objective function for PG-GMM learning and finally obtain the GMM model with learned parameters including mixture weights $\{\pi_k\}_{k=1}^K$, mean vectors $\{\boldsymbol{\mu}_k = \mathbf{0}\}_{k=1}^K$, and covariance matrices $\{\Sigma_k\}_{k=1}^K$. Noted that the mean vector of each cluster is natural zeros, i.e., $\boldsymbol{\mu}_k = \mathbf{0}$.

324 **3.2. External Prior Guided Internal Orthogonal**
 325 **Dictionary Learning**

327 Given a rael noisy image, we extract noisy PGs from it
 328 and save the mean vectors of each PG for recovering. The
 329 mean substracted PG is defined as $\bar{\mathbf{Y}}$. To project this PG
 330 into a most adaptive subspace, we select the most suitable
 331 Gaussian component to it from the PG-GMM trained in pre-
 332 vious section. The selection can be done by checking the
 333 posterior probability that $\bar{\mathbf{Y}}$ belongs to the k th Gaussian
 334 component:

$$P(k|\bar{\mathbf{Y}}) = \frac{\prod_{m=1}^M \mathcal{N}(\bar{\mathbf{y}}_m | \mathbf{0}, \Sigma_k)}{\sum_{l=1}^K \prod_{m=1}^M \mathcal{N}(\bar{\mathbf{y}}_m | \mathbf{0}, \Sigma_l)}. \quad (3)$$

338 Since the noise on real images are mostly small when com-
 339 pared to the signals, the covariance matrix of the k th com-
 340 ponent is still Σ_k . Finally, the component with the maxi-
 341 mum A-posteriori (MAP) probability $\ln P(k|\bar{\mathbf{Y}})$ is selected
 342 as the most suitable subspace for $\bar{\mathbf{Y}}$.

343 Though each PG has been projected into its most suitable
 344 subspace, the pre-learned subspace is still too general to
 345 represent the noisy PG extracted from the real noisy image.
 346 That is, the noisy PGs projected into one cluster can still
 347 constisted a subspace which is of lower dimensions than the
 348 subspace pre-learned from the external PGs. This can be
 349 demonstrated by compare the distribution of external PGs
 350 and internal PGs in the same clusters. We randomly select
 351 one cluster, and collect the celan PGs extracted from exter-
 352 nal dataset (Kodak 24 images) and the niosy PGs from the
 353 testing image. Since the original PGs are of $3p^2$ dimensions,
 354 we apply PCA to project the PGs into 2 dimensions for bet-
 355 ter visualization. The results is shown in Figure ??, from
 356 which we can see clearly that the projected PGs are mainly
 357 in a smaller region of the external PGs, which proves that
 358 the internal PGs are only consisted a subspace in a lower
 359 dimension than the PGs collected from external subspace.
 360 To better and adaptively charactering the internal PGs from
 361 the testing image, we need learn a more specific dictionary
 362 for noisy PGs assigned into each cluster. For notation sim-
 363 plicity, we ignore the index of subspace k . The internal PGs
 364 \mathbf{Y} form a subspace which can be obtained by singular value
 365 decomposition (SVD),

$$\begin{aligned} & \min_{\mathbf{D}_i \in \mathbb{R}^{3p^2 \times r}, \mathbf{A} \in \mathbb{R}^{3p^2 \times MN}} \|\mathbf{Y} - [\mathbf{D}_e \mathbf{D}_i] \mathbf{A}\|_F^2 + \lambda \|\mathbf{A}\|_1 \\ & \text{s.t. } \mathbf{D}_e^T \mathbf{D}_i = \mathbf{I}_r, \mathbf{D}_e^T \mathbf{D}_i = \mathbf{0}, \end{aligned} \quad (4)$$

370 The singular vectors capture the statistical structures of NSS
 371 variations in natural images, while the singular values in \mathbf{S}
 372 represent the significance of these singular vectors. Fig. 4
 373 shows the singular vectors for one Gaussian component.

374 **3.3. Optimization with Closed-form Solution**

376 Similar to the K-SVD [3], we employ an alternating it-
 377 erative framework to solve the optimization problem 4. In

378 fact, we initialize the orthogonal dictionary as $\mathbf{D}^{(0)}$ and for
 379 $t = 0, 1, \dots, T - 1$, alternatively do

380 **Updating Sparse Coefficients:** given the initialization
 381 orthogonal dictioanry $\mathbf{D}_i^{(t)}$, the sparce coefficients $\mathbf{A}^{(t)}$ are
 382 obtained via solving

$$\mathbf{A}^{(t)} := \arg \min_{\mathbf{A} \in \mathbb{R}^{3p^2 \times MN}} \|\mathbf{Y} - [\mathbf{D}_e \mathbf{D}_i^{(t)}] \mathbf{A}\|_F^2 + \lambda \|\mathbf{A}\|_1. \quad (5)$$

383 This problem has closed-form solution by $\mathbf{A}^* = T_\lambda(\hat{\mathbf{D}}^T \mathbf{Y})$, where $T_\lambda(\mathbf{A}) = \text{sgn}(\mathbf{A}) \odot \max(\mathbf{A}, \lambda)$ is a soft-
 384 thresholding function.

385 **Updating Orthogonal Dictionary:** given the sparse co-
 386 efficients $\mathbf{A}^{(0)}$, the sparce coefficients $\mathbf{A}^{(t)}$ are obtained via
 387 solving

$$\begin{aligned} \mathbf{D}_i^{(t+1)} &:= \arg \min_{\mathbf{D}_i \in \mathbb{R}^{3p^2 \times r}} \|\mathbf{Y} - [\mathbf{D}_e \mathbf{D}_i] \mathbf{A}^{(t)}\|_F^2 \\ &\text{s.t. } \mathbf{D}_i^T \mathbf{D}_i = \mathbf{I}_r, \mathbf{D}_e^T \mathbf{D}_i = \mathbf{0}, \end{aligned} \quad (6)$$

393 Dividing the sparse coefficients $\mathbf{A} = [\mathbf{A}_e^T \mathbf{A}_i^T]^T$, where \mathbf{A}_e
 394 and \mathbf{A}_i denote the coefficients over external and internal
 395 dictionary \mathbf{D}_e and \mathbf{D}_i . According to the Proposition 2.2
 396 in [33], the problem (6) has a closed-form solution $\mathbf{D}_i^* =$
 397 $\mathbf{U}\mathbf{V}^T$, where \mathbf{U} and \mathbf{V} are the orthogonal matrices obtained
 398 by the following SVD

$$(\mathbf{I} - \mathbf{D}_e \mathbf{D}_e^T) \mathbf{Y} \mathbf{A}_i^T = \mathbf{U} \Sigma \mathbf{V}^T \quad (7)$$

404 With these solutions, the final obtained dictionary $\mathbf{D} =$
 405 $[\mathbf{D}_e \mathbf{D}_i]$ are orthogonal ictionary. This can be proved by
 406 the following equation

$$\mathbf{D}^T \mathbf{D} = \begin{pmatrix} \mathbf{D}_e^T \\ \mathbf{D}_i^T \end{pmatrix} (\mathbf{D}_e \mathbf{D}_i) = \begin{pmatrix} \mathbf{D}_e^T \mathbf{D}_e & \mathbf{D}_e^T \mathbf{D}_i \\ \mathbf{D}_i^T \mathbf{D}_e & \mathbf{D}_i^T \mathbf{D}_i \end{pmatrix} = \mathbf{I} \quad (8)$$

413 **3.4. Discussion on External Prior and Internal Or-
 414 thogonal Dictionary Learning**

415 Until now, we have divided the noisy PGs into multiple
 416 internal subspaces. Here we take a deep analysis on how the
 417 external NSS prior guide the subspace learning of internal
 418 PGs. The help are at least threefold. Firstly, through MAP
 419 in (3), the external prior guides the noisy PGs to be clustered
 420 into the correct subspaces. If we cluster the noisy PGs in an
 421 automatical way, the subspaces we learned will be highly
 422 degraded by the signal dependent noise. Secondly, the guid-
 423 ance of external prior for internal clustering is more efficient
 424 than directly clustering the internal noisy PGs. It only needs
 425 to calculate the MAP probability via the equation (3) while
 426 the internal clustering via GMM is time-consuming on EM
 427 algorithm [34]. Thirdly, due to the correct guidance of ex-
 428 ternal prior, the structual decomposition via SVD of each
 429 subspace is more adaptive. This will bring better denois-
 430 ing performance than the methods only using the external

432 information. The *mutual incoherence* $\mu(\mathbf{U})$ [35], which is
 433 defined as

$$\mu(\mathbf{U}) = \max_{i=j} \frac{|\mathbf{d}_i^T \mathbf{d}_j|}{\|\mathbf{d}_i\|_2 \|\mathbf{d}_j\|_2} \quad (9)$$

, is a measure of quality of dictionary.

The Internal PGs are in fact lying in the subspaces of external PG Spaces. To defend this argument, we compare the distribution of external PGs extracted from clean natural images and real noisy images. For better illumination, we randomly selected a cluster and project the original clean PGs \mathbf{X} onto a 2-D plane. This could be done via $\mathbf{X}\mathbf{p} = \mathbf{U}(:, 1:2)^T \mathbf{X}$, where \mathbf{U} is the singular vector matrix of that cluster. The noisy PGs \mathbf{Y} assigned in this cluster is also projected into 2-D via $\mathbf{Y}\mathbf{p} = \mathbf{U}(:, 1:2)^T \mathbf{Y}$. The Figure ?? reflects the distribution on the 2-D plane of the projected clean PGs from external natural images and the projected noisy PGs from internal image. We can see that the internal noisy PGs are indeed lying in a subspace of the external PGs. Hence, if we directly use the external prior learned from clean PGs, the learned subspaces would be too generative to be suitable for the testing data.

Through SVD, the PGs in each internal subspace can be divided into singular vectors and singular values. The singular vectors are the basis of the corresponding subspace while the singular values reflect the importance of these basis. The basis can be used as dictionary to code the noisy PGs. And the singular values are adaptive parameters for internal noisy PGs. We can compare the singular values of one internal subspace and the corresponding space of external PGs. The result is shown in Figure ???. From which we can see that the noisy subspace often have higher values than external space consisted of clean PGs. This gap is clearly made of the noise and can be used for image denoising in a natural way.

4. The Denoising Algorithm

4.1. Fast Patch Group Searching by Integral Image

The searching of patch groups in images is inefficient if we search non-local similar patches to each local patch. To speed up the searching process and make our proposed method faster, we employ the technique of 'Summed Area Table' [36] for efficient PG searching. The SAT permits to evaluate the sum of pixel values in rectangular regions of the image with four operations, regardless of the region size. That is to say, we do not need do distance measure for each patch. It was first proposed under the name of summed area table[37]

4.2. Prior Weights for Sparse Coding

To remove the real noise, we employ the sparse coding framework. And in order to be adaptive to the input image, we employ the internal learned \mathbf{U} of each cluster as

Alg. 1: External Prior Guided Internal Orthogonal Dictionary Learning for Denoising Input: Noisy image \mathbf{y} , PG-GMM model 1. Initialization: $\hat{\mathbf{x}}^{(0)} = \mathbf{y}, \mathbf{y}^{(0)} = \mathbf{y};$ for $t = 1 : IteNum$ do for each PG \mathbf{Y} do 2. Calculate group mean μ_y and form PG $\bar{\mathbf{Y}}$; 3. Gaussian component selection via (3); end for for each Internal Subspace do 4. Internal Subspace Learning by (4); 5. Recover each patch in all PGs via $\hat{\mathbf{x}}_m = \mathbf{D}\hat{\alpha} + \mu_y$; end for 6. Aggregate the recovered PGs of all subspaces to form the recovered image $\hat{\mathbf{x}}^{(t)}$; end for Output: The recovered image $\hat{\mathbf{x}}^{(IteNum)}$.	486 487 488 489 490 491 492 493 494 495 496 497 498 499 500 501 502 503 504 505 506 507 508 509 510 511 512 513 514 515 516 517 518 519 520 521 522 523 524 525 526 527 528 529 530 531 532 533 534 535 536 537 538 539
---	--

an adaptive dictioanry to represent the structural variations of the PGs in that cluster. Since the \mathbf{U} is orthonormal, its *mutual incoherence* is naturally 0 and therefore better than other redundant dictionaries.

$$\min_{\boldsymbol{\alpha}} \|\bar{\mathbf{y}}_m - \mathbf{U}\boldsymbol{\alpha}\|_2^2 + \sum_{i=1}^{3p^2} \lambda_i |\alpha_i|. \quad (10)$$

The i th entry of the regularization parameter λ_i

$$\lambda_i = \lambda / (\mathbf{S}_i + \varepsilon), \quad (11)$$

where ε is a small positive number to avoid dividing by zero. Since the dictionary \mathbf{U} is orthonormal, it is not difficult to find out that (4) has a closed-form solution (detailed derivation can be found in the supplementary material):

$$\hat{\boldsymbol{\alpha}} = \text{sgn}(\mathbf{U}^T \bar{\mathbf{y}}_m) \odot \max(|\mathbf{U}^T \bar{\mathbf{y}}_m| - \boldsymbol{\Lambda}, \mathbf{0}), \quad (12)$$

where $\boldsymbol{\Lambda} = [\lambda_1, \lambda_2, \dots, \lambda_{3p^2}]$ is the vector of regularization parameter and $\text{sgn}(\bullet)$ is the sign function, \odot means element-wise multiplication, and $|\mathbf{U}^T \bar{\mathbf{y}}_m|$ is the absolute value of each entry of vector $|\mathbf{U}^T \bar{\mathbf{y}}_m|$. The closed-form solution makes our weighted sparse coding process very efficient.

4.3. The Overall Algorithm

With the solution $\hat{\boldsymbol{\alpha}}$ in (7), the clean patch in a PG can be estimated as $\hat{\mathbf{x}}_m = \mathbf{D}\hat{\boldsymbol{\alpha}} + \mu_y$. Then the clean image $\hat{\mathbf{x}}$ can be reconstructed by aggregating all the estimated PGs. In practice, we could perform the above denoising procedures for several iterations for better denoising outputs. In iteration t , we use the iterative regularization strategy [38] to add back to the recovered image $\hat{\mathbf{x}}^{(t-1)}$ some estimation residual in iteration $t-1$. The proposed denoising algorithm is summarized in Algorithm 1 (Alg. 1).



Figure 2. Some testing images in the dataset [13].



Figure 3. Some cropped images of the dataset [13].

5. Experiments

In this section, we perform real image denoising experiments on three standard datasets. The first dataset is real noisy images with mean images as ground truths provided by [13], some samples are shown in Figure 3. The second dataset is provided by the website of Noise Clinic [18]. The third dataset is provided by the Commercial software Neat Image [23]. The second and third dataset do not have ground truth images.

5.1. Implementation Details

Our proposed method contains two stages, the external prior guided internal subspace learning stage and the adaptive denoising stage. In the learning stage, there are 4 parameters: the patch size p , the number of patches in a PG M , the window size W for PG searching and the number of clusters K . We set $p = 6$ (hence the patch size is $6 \times 6 \times 3$), $M = 10$, $W = 31$, $K = 32$. We extracted about 3.6 million PGs from the Kodak PhotoCD Dataset, which includes 24 high quality color images, to train the external prior via PG-GMM. In the denoising stage, the parameter $\lambda = 0.002$ is used to regularize the sparse term. The δ in iterative regularization is set as $\delta = 0.09$.

5.2. Comparison on External and Internal methods

In this subsection, we compared the proposed external prior guided internal subspace learning model on real image denoising. The three methods are evaluated on the dataset provided in [13]. We calculate the PSNR, SSIM [21] and visual quality of these three methods. We also compare the speed. The PSNR and SSIM results on 60 cropped images from [13] are listed in Table 1. The images are cropped into size of 500×500 for better illustration. We also compare the three methods on visual quality in Figure 5.2. Compare the denoised images listed in Figure 5.2 and Figure 5.2, we

Table 1. Average PSNR(dB)/SSIM results of external, internal, and guided methods on 60 cropped real noisy images in [13].

	Noisy	Offline	Online	Guided
PSNR	34.51	38.19	38.07	38.55
SSIM	0.8718	0.9663	0.9625	0.9675

can see that the Offline method is better at edges, smooth regions while the Online method is good at complex textures. The reason is two folds. Firstly, the Offline method is learned on clean images and hence is better at representing edges, structures, and smooth area. The online method is influenced by the noise and hence some noise cannot be removed. Secondly, the Online method is better at recovering complex area since they could learn adaptive dictionaries for the specific area. The Offline method cannot recover the complex area since they did not learn the similar structures from the external natural clean images.

5.3. Comparison With other Competing Methods

We compare with previous state-of-the-art Gaussian noise removal methods such as BM3D [4], WNNM [8], MLP [7], CSF [9], and the recently proposed TRD [11]. We also compare with three competing real image denoising methods such as Noise Clinic, Neat Image, and the CCNoise method proposed recently. The popular software NeatImage which is one of the best denoising software available. All these methods need noise estimation which is very hard to perform if there is no uniform regions available in the testing image. The NeatImage will fail to perform automatical parameters settings if there is no uniform regions.¹

We the competing denoising methods from various research directions on two datasets. Both the two datasets comes from the [13]. The first dataset contains 17 images of size over 7000×5000 . Since this dataset contains repetitive contents across different images, we crop 60 small images of size 500×500 from these 17 images in [13].

The PSNR and SSIM results are listed in Table 3. The number in red color and blue color means the best and second best results, respectively. From the Table 3, we can see that the external based method can already surpass largely the previous denoising methods. The improvement on PSNR over the second best method, i.e., TRD, is 0.44dB. The

5.4. Discussion on Parameter λ

The proposed method only has a key parameter, namely the regularization parameter λ . To demonstrate that the proposed method is robust to the variance of λ , we vary the

¹To compare with CCNoise, we first transform the denoised images into double format.

648

649

650

651

652

653

654

655

656

657

658

659

660

661

662

663

664

665

666

667

668

669

670

671

672

673

674

675

676

677

678

679

680

681

682

683

684

685

686

687

688

689

690

691

692

693

694

695

696

697

698

699

700

701

702

703

704

705

706

707

708

709

710

711

712

713

714

715

716

717

718

719

720

721

722

723

724

725

726

727

728

729

730

731

732

733

734

735

736

737

738

739

740

741

742

743

744

745

746

747

748

749

750

751

752

753

754

755



Figure 4. Denoised images of the image "Nikon D600 ISO 3200 C1" by different methods. The images are better to be zoomed in on screen.

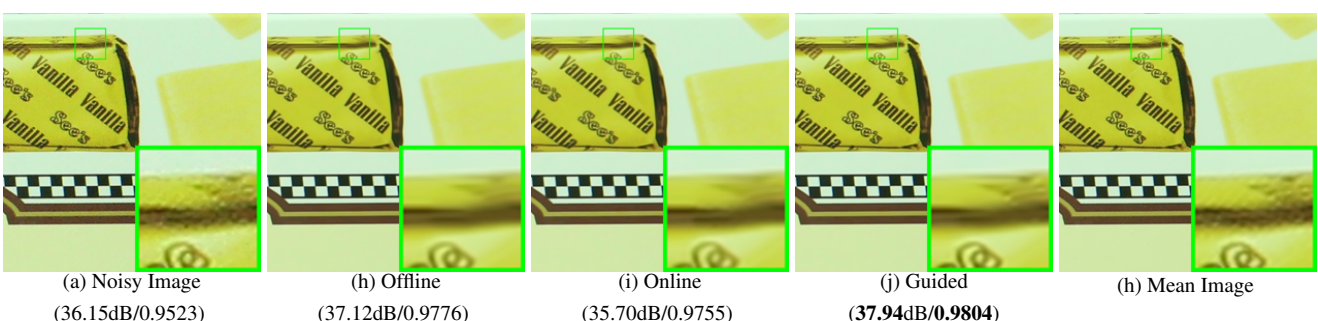


Figure 5. Denoised images of the image "Canon EOS 5D Mark3 ISO 3200 C1" by different methods. The images are better to be zoomed in on screen.

parameter λ across a wide range and obtain the PSNR and SSIM results as a function of the parameter λ . The results is shown in Figure 8, from which we can see that the proposed method can achieve a PSNR (SSIM) over 38.5dB (0.9660) when λ varies from 0.0015 to 0.0025. This shows that the proposed method is indeed robust to the chosen of the paramter λ .

6. Conclusion and Future Work

In the future, we will evaluate the proposed method on other computer vision tasks such as single image super-resolution, photo-sketch synthesis, and cross-domain image recognition. Our proposed method can be improved if we use better training images, fine tune the parameters via cross-validation. We believe that our framework can be useful not just for real image denoising, but for image super-resolution, image cross-style synthesis, and recognition tasks. This will be our line of future work.

References

- [1] A. Buades, B. Coll, and J. M. Morel. A non-local algorithm for image denoising. *CVPR*, pages 60–65, 2005. [1](#), [2](#), [3](#)
- [2] S. Roth and M. J. Black. Fields of Experts. *International Journal of Computer Vision*, 82(2):205–229, 2009. [1](#)
- [3] M. Elad and M. Aharon. Image denoising via sparse and redundant representations over learned dictionaries. *Image Processing, IEEE Transactions on*, 15(12):3736–3745, 2006. [1](#), [3](#), [4](#)
- [4] K. Dabov, A. Foi, V. Katkovnik, and K. Egiazarian. Image denoising by sparse 3-D transform-domain collaborative filtering. *Image Processing, IEEE Transactions on*, 16(8):2080–2095, 2007. [1](#), [2](#), [3](#), [6](#)
- [5] J. Mairal, F. Bach, J. Ponce, G. Sapiro, and A. Zisserman. Non-local sparse models for image restoration. *ICCV*, pages 2272–2279, 2009. [1](#), [2](#), [3](#)
- [6] D. Zoran and Y. Weiss. From learning models of natural image patches to whole image restoration. *ICCV*, pages 479–486, 2011. [1](#), [2](#)
- [7] Harold C Burger, Christian J Schuler, and Stefan Harmeling. Image denoising: Can plain neural networks compete with bm3d? *Computer Vision and Pattern Recognition (CVPR), 2012 IEEE Conference on*, pages 2392–2399, 2012. [1](#), [2](#), [3](#), [6](#)
- [8] S. Gu, L. Zhang, W. Zuo, and X. Feng. Weighted nuclear norm minimization with application to image denoising. *CVPR*, pages 2862–2869, 2014. [1](#), [2](#), [3](#), [6](#)
- [9] U. Schmidt and S. Roth. Shrinkage fields for effective image restoration. *Computer Vision and Pattern Recognition (CVPR), 2014 IEEE Conference on*, pages 2774–2781, June 2014. [1](#), [2](#), [3](#), [6](#)
- [10] J. Xu, L. Zhang, W. Zuo, D. Zhang, and X. Feng. Patch group based nonlocal self-similarity prior learning for image denoising. *2015 IEEE International Conference on Computer Vision (ICCV)*, pages 244–252, 2015. [1](#), [2](#), [3](#)

756 Table 2. Average PSNR(dB) results of different methods on 60 cropped real noisy images captured in [13].
757

810

	Noisy	CBM3D	WNNM	MLP	CSF	TRD	NI	NC	Guided	Guided2
PSNR	34.51	34.58	34.52	36.19	37.40	37.75	36.53	37.57	38.72	38.90
SSIM	0.8718	0.8748	0.8743	0.9470	0.9598	0.9617	0.9241	0.9514	0.9694	0.9702

811

812

813

814

815

816

817

818

819

820

821

822

823

824

825

826

827

828

829

830

831

832

833

834

835

836

837

838

839

840

841

842

843

844

845

846

847

848

849

850

851

852

853

854

855

856

857

858

859

860

861

862

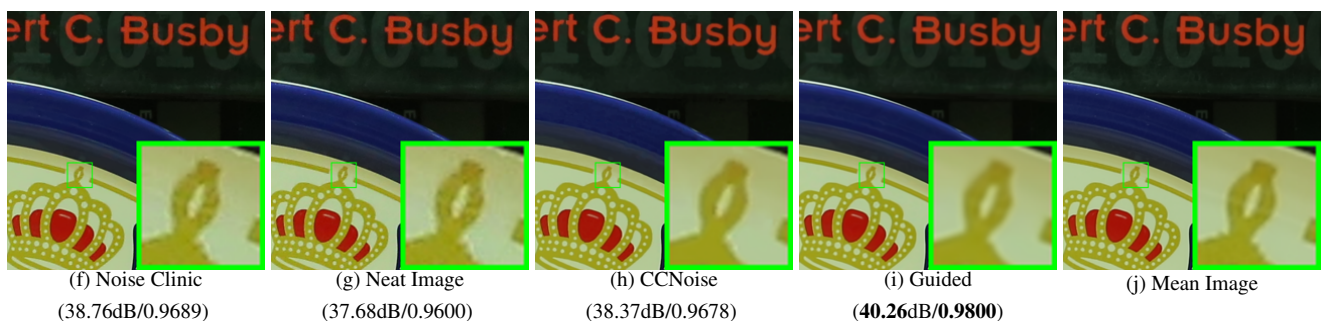
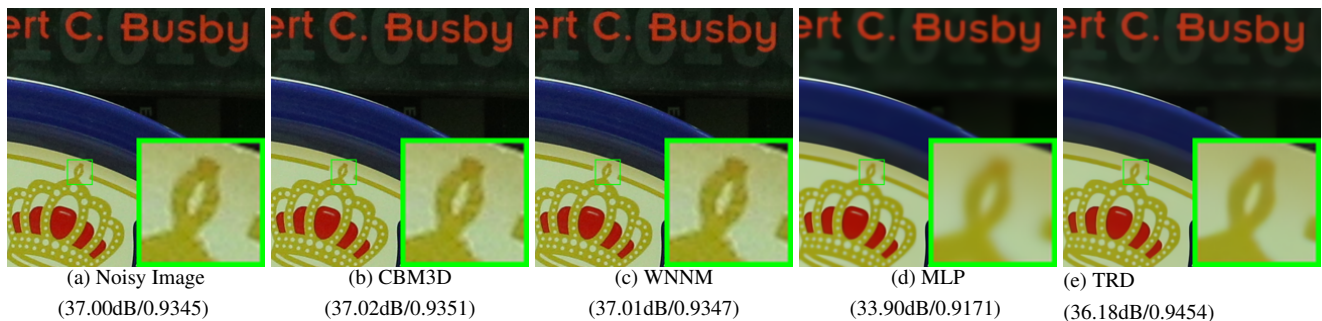
863

761 Table 3. Average PSNR(dB) results of different methods on 15 cropped real noisy images used in [13].
762

Camera Settings	Noisy	CBM3D	WNNM	MLP	CSF	TRD	NI	NC	CC	Guided2
Canon 5D Mark III ISO = 3200	37.00	37.08	37.09	33.92	35.68	36.20	37.68	38.76	38.37	40.50
	33.88	33.94	33.93	33.24	34.03	34.35	34.87	35.69	35.37	37.22
	33.83	33.88	33.90	32.37	32.63	33.10	34.77	35.54	34.91	37.13
Nikon D600 ISO = 3200	33.28	33.33	33.34	31.93	31.78	32.28	34.12	35.57	34.98	35.34
	33.77	33.85	33.79	34.15	35.16	35.34	35.36	36.70	35.95	36.69
	34.93	35.02	34.95	37.89	39.98	40.51	38.68	39.28	41.15	39.17
Nikon D800 ISO = 1600	35.47	35.54	35.57	33.77	34.84	35.09	37.34	38.01	37.99	38.82
	35.71	35.79	35.77	35.89	38.42	38.65	38.57	39.05	40.36	40.98
	34.81	34.92	34.95	34.25	35.79	35.85	37.87	38.20	38.30	38.90
Nikon D800 ISO = 3200	33.26	33.34	33.31	37.42	38.36	38.56	36.95	38.07	39.01	38.69
	32.89	32.95	32.96	34.88	35.53	35.76	35.09	35.72	36.75	36.82
	32.91	32.98	32.96	38.54	40.05	40.59	36.91	36.76	39.06	38.80
Nikon D800 ISO = 6400	29.63	29.66	29.71	33.59	34.08	34.25	31.28	33.49	34.61	33.31
	29.97	30.01	29.98	31.55	32.13	32.38	31.38	32.79	33.21	33.18
	29.87	29.90	29.95	31.42	31.52	31.76	31.40	32.86	33.22	33.35
Average PSNR	33.41	33.48	33.48	34.32	35.33	35.65	35.49	36.43	36.88	37.26
Average SSIM	0.8483	0.8511	0.8512	0.9113	0.9250	0.9280	0.9126	0.9364	0.9481	0.9505

- [11] Yunjin Chen, Wei Yu, and Thomas Pock. On learning optimized reaction diffusion processes for effective image restoration. *Proceedings of the IEEE Conference on Computer Vision and Pattern Recognition*, pages 5261–5269, 2015. 1, 2, 3, 6
- [12] S. J. Kim, H. T. Lin, Z. Lu, S. Ssstrunk, S. Lin, and M. S. Brown. A new in-camera imaging model for color computer vision and its application. *IEEE Transactions on Pattern Analysis and Machine Intelligence*, 34(12):2289–2302, Dec 2012. 1
- [13] Seonghyeon Nam, Youngbae Hwang, Yasuyuki Matsushita, and Seon Joo Kim. A holistic approach to cross-channel image noise modeling and its application to image denoising. *Proc. Computer Vision and Pattern Recognition (CVPR)*, pages 1683–1691, 2016. 1, 3, 6, 8
- [14] J. Portilla. Full blind denoising through noise covariance estimation using gaussian scale mixtures in the wavelet domain. *Image Processing, 2004. ICIP '04. 2004 International Conference on*, 2:1217–1220, 2004. 1, 3
- [15] Tamer Rabie. Robust estimation approach for blind denoising. *Image Processing, IEEE Transactions on*, 14(11):1755–1765, 2005. 1, 3
- [16] C. Liu, R. Szeliski, S. Bing Kang, C. L. Zitnick, and W. T. Freeman. Automatic estimation and removal of noise from a single image. *IEEE Transactions on Pattern Analysis and Machine Intelligence*, 30(2):299–314, 2008. 1, 3

- [17] Zheng Gong, Zuowei Shen, and Kim-Chuan Toh. Image restoration with mixed or unknown noises. *Multiscale Modeling & Simulation*, 12(2):458–487, 2014. 1, 3
- [18] M. Lebrun, M. Colom, and J.-M. Morel. Multiscale image blind denoising. *Image Processing, IEEE Transactions on*, 24(10):3149–3161, 2015. 1, 2, 3, 6
- [19] Fengyuan Zhu, Guangyong Chen, and Pheng-Ann Heng. From noise modeling to blind image denoising. *The IEEE Conference on Computer Vision and Pattern Recognition (CVPR)*, June 2016. 1, 3
- [20] C. M. Bishop. *Pattern recognition and machine learning*. New York: Springer, 2006. 1, 3
- [21] Z. Wang, A. C. Bovik, H. R. Sheikh, and E. P. Simoncelli. Image quality assessment: from error visibility to structural similarity. *IEEE Transactions on Image Processing*, 13(4):600–612, 2004. 1, 6
- [22] K. Dabov, A. Foi, V. Katkovnik, and K. Egiazarian. Color image denoising via sparse 3d collaborative filtering with grouping constraint in luminance-chrominance space. *IEEE International Conference on Image Processing*, 1, 2007. 2
- [23] Neatlab ABSsoft. Neat image. <https://neatvideo.com/home>. 2, 6
- [24] Glenn E Healey and Raghava Kondepudy. Radiometric ccd camera calibration and noise estimation. *IEEE Transactions on Pattern Analysis and Machine Intelligence*, 16(3):267–276, 1994. 1, 3



885 Figure 6. Denoised images of the image "Canon 5D Mark 3 ISO 3200 1" by different methods. The images are better to be zoomed in on screen.



910 Figure 7. Denoised images of the image "5dmak3iso32003" by different methods. The images are better to be zoomed in on screen.

913 [25] Daniel Glasner, Shai Bagon, and Michal Irani. Super-
914 resolution from a single image. *ICCV*, 2009. 2

915 [26] Maria Zontak, Inbar Mosseri, and Michal Irani. Separating
916 signal from noise using patch recurrence across scales. *Pro-*

ceedings of the IEEE Conference on Computer Vision and Pattern Recognition, pages 1195–1202, 2013. 2

[27] Tomer Michaeli and Michal Irani. Blind deblurring using internal patch recurrence. *European Conference on Computer*

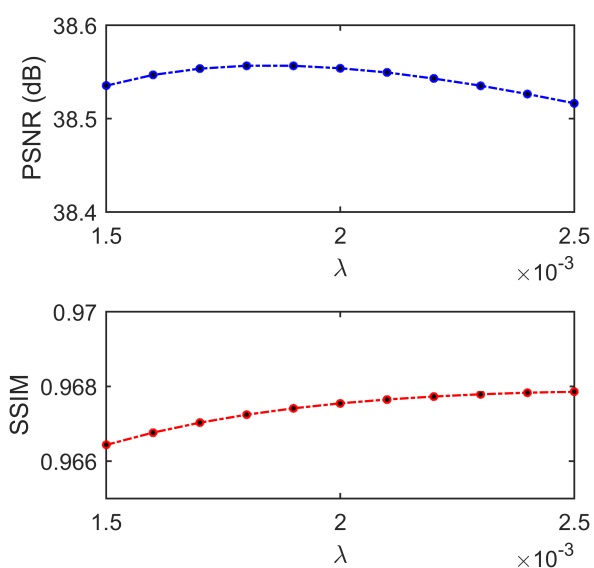


Figure 8. The PSNR/SSIM results as a function of the parameter λ .

Vision, pages 783–798, 2014. 2

- [28] Y. Bahat and M. Irani. Blind dehazing using internal patch recurrence. *IEEE International Conference on Computational Photography (ICCP)*, pages 1–9, May 2016. 2
- [29] J. Portilla, V. Strela, M.J. Wainwright, and E.P. Simoncelli. Image denoising using scale mixtures of Gaussians in the wavelet domain. *Image Processing, IEEE Transactions on*, 12(11):1338–1351, 2003. 3

- [30] Peter J Huber. *Robust statistics*. Springer, 2011. 3

- [31] M. Lebrun, A. Buades, and J. M. Morel. A nonlocal bayesian image denoising algorithm. *SIAM Journal on Imaging Sciences*, 6(3):1665–1688, 2013. 3

- [32] W. Dong, L. Zhang, G. Shi, and X. Li. Nonlocally centralized sparse representation for image restoration. *Image Processing, IEEE Transactions on*, 22(4):1620–1630, 2013. 3

- [33] Chenglong Bao, Jian-Feng Cai, and Hui Ji. Fast sparsity-based orthogonal dictionary learning for image restoration. *Proceedings of the IEEE International Conference on Computer Vision*, pages 3384–3391, 2013. 4

- [34] A. P. Dempster, N. M. Laird, and D. B. Rubin. Maximum likelihood from incomplete data via the EM algorithm. *Journal of the Royal Statistical Society. Series B (methodological)*, pages 1–38, 1977. 4

- [35] David L Donoho and Michael Elad. Optimally sparse representation in general (nonorthogonal) dictionaries via 1 minimization. *Proceedings of the National Academy of Sciences*, 100(5):2197–2202, 2003. 5

- [36] Franklin C. Crow. Summed-area tables for texture mapping. *SIGGRAPH Comput. Graph.*, 18(3):207–212, January 1984. 5

- [37] Paul Viola and Michael J Jones. Robust real-time face detection. *International journal of computer vision*, 57(2):137–154, 2004. 5

- [38] S. Osher, M. Burger, D. Goldfarb, J. Xu, and W. Yin. An iterative regularization method for total variation-based image restoration. *Multiscale Modeling & Simulation*, 4(2):460–489, 2005. 5

1026

1027

1028

1029

1030

1031

1032

1033

1034

1035

1036

1037

1038

1039

1040

1041

1042

1043

1044

1045

1046

1047

1048

1049

1050

1051

1052

1053

1054

1055

1056

1057

1058

1059

1060

1061

1062

1063

1064

1065

1066

1067

1068

1069

1070

1071

1072

1073

1074

1075

1076

1077

1078

1079